EPR Spectroscopy of Impurity Ytterbium Ions in Synthetic Forsterite Single Crystals

V. F. Tarasov[1] · **A. A. Sukhanov**[1] · **E. V. Zharikov**[2] · **K. A. Subbotin**[2,3] · **D. A. Lis**[2]

Abstract

Continuous wave and pulse X-band electron paramagnetic resonance spectroscopy are used to determine structure, magnetic and relaxation properties of paramagnetic centers formed by impurity ytterbium ions in forsterite (Mg_2SiO_4) single crystals. It is found that Yb^{3+} ions substitute Mg^{2+} ions both as single ions and as dimeric associates with nearby magnesium vacancy. For all ytterbium centers, magnetic properties are characterized by the strong easy plane anisotropy. Measurements in temperature range 5–15 K showed that spin–lattice relaxation of the Yb^{3+} ions in Mg_2SiO_4 is due to joint action of direct one-phonon process, Raman two-phonon process and resonance two-phonon Aminov–Orbach process.

1 Introduction

Rare-earth impurity ions in crystals are widely studied as possible material basis for practical implementation of information technologies based on the laws of quantum mechanics. Among them, they are quantum calculations, quantum telecommunications and quantum memory. Magnetic and relaxation properties of electron–nuclear spin systems of impurity rare-earth ions in crystals are actively studied [1–7] as promising materials allowing the reversible transform of quantum states between photons and nuclear spins used as a long-lived quantum memory units. Possibilities of using the electron spins of rare-earth ions as quantum bits (qubits) for quantum calculation were investigated in Refs. [8, 9]. To implement elementary quantum calculations, at least two coupled qubits are required. Various practical implementations of such qubits based on electron spins are proposed in Refs. [10–13]. Dimeric

✉ V. F. Tarasov
  tarasov@kfti.knc.ru

1   Zavoisky Physical-Technical Institute, Federal Research Center "Kazan Scientific Center
   of RAS", Kazan 420029, Russia

2   Prokhorov General Physics Institute, Russian Academy of Sciences, Moscow 119991, Russia

3   Mendeleev University of Chemical Technology, Moscow 125047, Russia

associates of impurity ions in dielectric crystals were not considered up to now as promising basis for the two qubits quantum calculations. The reason for this fact is that doped crystals should be magnetically diluted for efficient reduction of decoherence because of spin–spin interaction. And it is commonly assumed that at low impurity concentration, the relative probability of the formation of dimeric associates is very low. Therefore, it is of interest to study crystals where distribution of impurity ions in crystal lattice is not statistical, but effect of dimeric self-organization of impurity ions occurs. In case of heterovalent substitution of divalent cation by trivalent impurity ion, a compensator for the excess cationic charge is required. If such compensator is not specially introduced into the crystal during the crystal growth, the charge compensation occurs via the internal charged point defects, first, by divalent cation vacancies. Moreover, since such vacancies and trivalent impurity ions have the opposite charges, they trend to form associates, consisting, in particular, of two impurity ions and one vacancy of divalent ion located in three closely neighboring magnesium sites. Then the total cationic charge is preserved, and such associates bring a minimal increase of the internal energy of the crystal lattice. As a result, trivalent impurity ions are characterized by a pronounced effect of dimeric self-organization, results in the aggregation of impurity ions into dimeric associates during the crystals growth. The concentration of these associates may be nearly the same or even exceed the concentration of the single ions. This effect was found for trivalent ytterbium in $CsCdBr_3$ [14, 15] and forsterite Mg_2SiO_4 [16]. We observed this effect in forsterite also for chromium [17], holmium [18], terbium [19] and erbium [20] ions. In this paper, continuous wave and pulsed electron paramagnetic resonance (EPR) spectroscopy is used to study magnetic and relaxation characteristics of paramagnetic centers formed by ytterbium impurity ions in Mg_2SiO_4 single crystals.

2 Experimental (Objects and Methods)

Crystal structure of forsterite was described in Ref. [21]. A unit cell of forsterite crystalline structure has an orthorhombic symmetry with a space group *Pbnm* (the lattice constants equal $a = 0.4753$, $b = 1.019$, $c = 0.5988$ nm) and contains 4 formula units. Ytterbium ions can substitute magnesium ions located in two sites inside two structurally nonequivalent oxygen octahedra denoted M1 and M2. The M1 octahedra form a quasi-one-dimensional chain oriented along the crystal *c*-axis. The M2 octahedra are adjacent to this chain from the sides. Projection of oxygen M1 and M2 octahedra onto the (*bc*) plane is presented in Fig. 1. Preliminary results of EPR study of ytterbium substituting magnesium in the M1 site as single ion and dimeric associate were presented in Ref. [16]. Most probable structure of the dimeric associates was determined in Ref. [22] by structure computer simulation of various possible clusters of ytterbium centers by the method of interatomic potentials with the GULP 4.0.1 code (General Utility Lattice Program) [23]. It was established that it consists of two ytterbium ions and magnesium vacancy between them substituting three magnesium ions in the M1 sites forming a chain parallel to the *c* crystallographic axis. This structure is highlighted by bold lines in the right side of the figure.
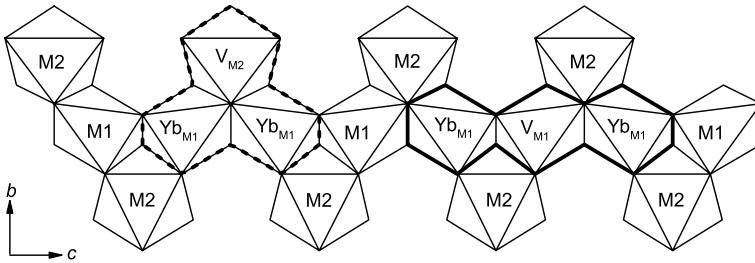
Fig. 1 Projection of oxygen octahedra of the Mg_2SiO_4 structure onto the (*bc*) plane and possible structures of dimeric associates of ytterbium ions localized in the M1 sites (Yb_{M1}). V_{M1} and V_{M2}—magnesium vacancies in the M1 and M2 sites

The crystal field in the M1 site has inversion symmetry with the C_i point symmetry. The principal magnetic axes of paramagnetic centers in the M1 sites deviate from the crystallographic planes, and at arbitrary orientation of an external magnetic field there are 4 magnetically nonequivalent M1 sites. If the external magnetic field lies in the crystallographic planes, two out of four nonequivalent centers become equivalent. The crystal field in the M2 site with the C_s point symmetry has a mirror symmetry plane perpendicular to the *c*-axis. Therefore, there are only 2 magnetically nonequivalent centers for the paramagnetic centers in the M2 sites. The principal magnetic axes of these centers should be parallel to the *c*-axis or lie in the (*ab*) plane. If the external magnetic field lies in the (*ac*) or (*bc*) crystallographic planes, two nonequivalent centers become equivalent. This difference makes it possible to unambiguously distinguish centers located in M1 and M2 sites on the basis of orientation dependences of EPR spectra.

Mg_2SiO_4:Yb^{3+} single crystals were grown by the Czochralski technique in nitrogen atmosphere from the melt containing 0.05, 0.15 and 0.5 at. % of ytterbium in respect to Mg^{2+} (samples 1, 2 and 3, respectively). The growth was carried out from an iridium crucible on a single-crystal Mg_2SiO_4 seed that was cut along the *a* axis. The pulling rate at the nominal growth stage was 1 mm/h, and the rotation rate was 6 rot/min. Orientation of the crystals relative to the crystallographic axes for EPR measurements was determined by X-ray diffractometry. Samples for EPR measurements were cut in a cubic shape with dimensions $3 \times 3 \times 3$ mm. Samples faces were oriented parallel to crystallographic planes.

The crystal–melt partition coefficient of rare-earth impurity in forsterite is quite small and depends on the concentration of impurity ion [24]. We measured the actual concentration of ytterbium in the crystal for the sample 3 by means of induction-coupled plasma mass spectrometry. It was determined to be 1.06×10^{-3} wt%, or 4.34×10^{-4} at.% in respect to magnesium. Therefore, the crystal–melt partition coefficient of Yb in forsterite can be evaluated as 0.0009, which is lower than the value given in Ref. [24].

The concentration of ytterbium in the other two samples was estimated from the optical absorption spectra. Unpolarized optical absorption spectra of samples 1, 2, and 3 measured along the *a* axis of the crystals are presented in Fig. 2. There are the series of lines relating to impurity ytterbium ions, the strongest ones are at the
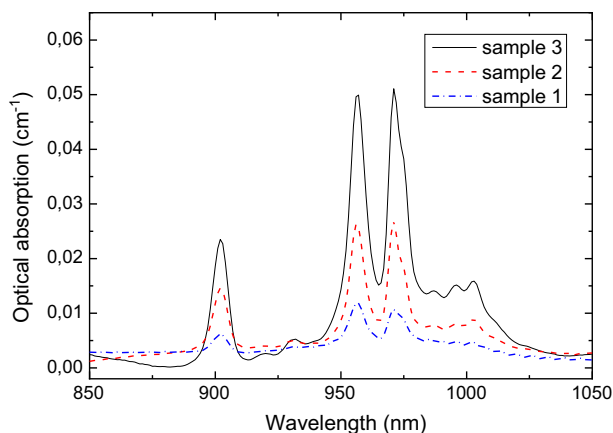
Fig. 2 Unpolarized optical absorption spectra of Mg_2SiO_4 single crystals doped with ytterbium and grown at ytterbium concentrations in the melt of 0.05, 0.15 and 0.5 mol.% (samples 1, 2 and 3, respectively)

wavelengths of 902, 956, and 971 nm. The ratio of the intensities of the absorption lines is 1:0.48:0.15 for the samples 3, 2 and 1, respectively. Since intensities of these lines are proportional to the actual contents of ytterbium in the crystals we estimated actual concentration of ytterbium in the samples 2 and 1 as 2.08×10^{-4} at.% and 6.51×10^{-5} at.%, respectively. Besides that, the peak absorption cross sections of Yb^{3+} lines in forsterite crystal can be calculated. For the strongest line at 971 nm, it is equal to 3.8×10^{-19} cm^2.

EPR measurements were carried out in the X-band on ELEXSYS E680 spectrometer with a cylindrical dielectric resonator ER4118MD5-W1 of the Flexline series. Continuous wave (CW) spectra were recorded at 15 K. Relaxation measurements were carried out in the temperature range of 5–15 K. All EPR measurements except direct comparison of results for different samples were carried out with the sample 2.

3 Results of CW EPR Spectroscopy

EPR spectra of Yb^{3+} ions in Mg_2SiO_4 are characterized by strong anisotropy. Figure 3 shows the orientation dependences of positions of the resonance lines on orientation of the external magnetic field in the (*bc*) and (*ab*) planes. It is seen in Fig. 3a that the orientation dependences of resonance lines are divided into two groups. For the first group, the orientations of the extreme positions of magnetic field differ from the crystallographic axes. Consequently, this group of lines belongs to ytterbium in the crystallographic M1 sites which have no elements of symmetry, except the inversion center. Transitions presented by black circles are due to single Yb^{3+} ions in four magnetically nonequivalent M1 sites. Four pairs of transitions presented by red squares are due to four nonequivalent dimeric associates formed by Yb^{3+} ions substituting two magnesium ions in magnetically equivalent M1 sites
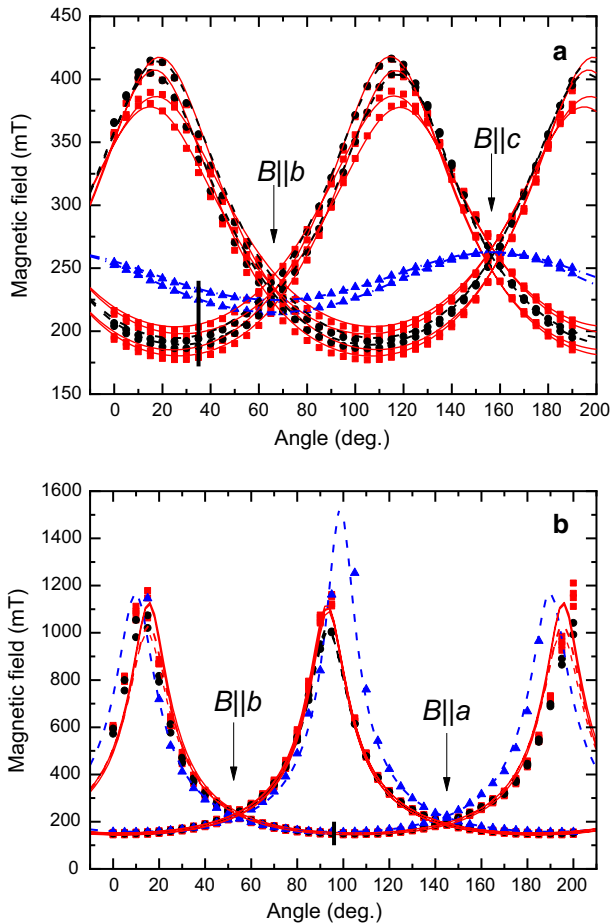
Fig. 3 Dependences of the resonance values of external magnetic field on the field orientation in the crystallographic planes. **a**, **b** (*bc*) and (*ab*) planes, respectively. Black circles, red squares and blue triangles are experimental data for the single Y^{3+} ion in the M1 site dimeric associate and center 3, respectively. Dashed and solid lines are fit to the spin Hamiltonians (2) and (3) for single ions and dimeric associates, respectively

[16]. For the second group of lines (blue triangles), the extreme positions of resonance fields coincide with the crystallographic axes. This is typical for a paramagnetic center in the M2 site, whose crystal field has the (*ab*) mirror plane of symmetry. We will designate this center as C3. Orientation dependences of positions of the resonance lines on orientation of the external magnetic field in the (*ab*) plane are presented in Fig. 3b. In this case orientation, dependences of all the observed paramagnetic centers are very similar. At the figure scale, the dependences for the single Yb^{3+} ion in the M1 sites and the dimeric associate of the Yb^{3+} ions are almost indistinguishable. Orientation dependence of the C3 center in this plane is slightly different from that of the Yb^{3+} ions in the M1 sites. There is a visible deviation

of the orientation dependences from the mirror symmetry for the two magnetically nonequivalent C3 centers. This deviation is due to deviation of the sample rotation axis from the crystallographic axis. We used the EasySpin program package [25] to determine the characteristics of paramagnetic centers formed by impurity Yb^{3+} ions in Mg_2SiO_4. Effective spin Hamiltonian of single ions was corresponded to the Zeeman interaction of effective electron spin $S = \frac{1}{2}$ with the external magnetic field $\mathbf{B}$

$$H_i = \beta(\mathbf{B} \cdot \mathbf{g} \cdot \mathbf{S}). \tag{1}$$

The spin Hamiltonian of the dimeric associate was represented by the sum of the Zeeman energies of two Yb^{3+} ions and the term corresponding to the spin–spin interaction between them.

$$H = H_1 + H_2 + \mathbf{S}_1 \cdot \mathbf{J} \cdot \mathbf{S}_2. \tag{2}$$

Here H_1 and H_2 are the spin Hamiltonians (1) for the two neighboring Yb^{3+} ions, the third term describes spin–spin interaction. When calculating, we assumed that both Yb^{3+} ions of the dimeric associate are localized in the same magnetically equivalent positions. The best agreement of the calculation with the experimental data was obtained with the parameters of the spin Hamiltonians (1) and (2) presented in Table 1. Lines in Fig. 3 are calculated with these parameters.

Euler angles $\alpha(g)$, $\beta(g)$, $\gamma(g)$, $\alpha(J)$, $\beta(J)$, $\gamma(J)$ determine orientations of principal axes of $\mathbf{g}$ and $\mathbf{J}$ tensors in the system of crystal axes (*zyz* convention). These angles correspond to one of the possible magnetically nonequivalent centers. Euler angles for the other centers can be determined taking into account mirror symmetry of magnetic properties of the centers relative to crystallographic planes.

During all our orientational measurements, the axis of the sample rotation did not coincide with the crystallographic axes. Noticeable asymmetry of orientational dependences of two nonequivalent C3 centers due to this deviation is

Table 1 Spin Hamiltonian parameters for the impurity Yb^{3+} ions in Mg_2SiO_4

Parameter	M1 single ion	M1 dimeric associate	C3 center
g_x	4.9 ± 0.1	5.0 ± 0.1	4.5 ± 0.1
g_y	2.0 ± 0.1	2.1 ± 0.1	2.6 ± 0.1
g_z	0.6 ± 0.1	0.6 ± 0.1	0.3 ± 0.1
$\alpha(g)$ (deg.)	67 ± 5	67 ± 5	90
$\beta(g)$ (deg.)	82 ± 5	83 ± 5	90
$\gamma(g)$ (deg.)	54 ± 5	53 ± 5	45 ± 5
J_x (MHz)		28 ± 10	
J_y (MHz)		564 ± 10	
J_z (MHz)		-798 ± 10	
$\alpha(J)$ (deg.)		110 ± 10	
$\beta(J)$ (deg.)		51 ± 10	
$\gamma(J)$ (deg.)		91 ± 10	

clearly seen in Fig. 3b. Essential difference between two centers that should be equivalent if the external magnetic field lies in the (*bc*) plane is clearly seen in Fig. 3a. Moreover, the value of this difference is comparable to the splitting due to spin–spin interaction between ytterbium ions in dimeric associate. Fittings of experimental data for Ref. [16] were done using the averaged values of resonance magnetic field without taking into account these deviations. This led to erroneous fitting results in Ref. [16]. Fitting for this article was carried out with taking into account existing inclining. Therefore, the data given in this article are more correct.

To determine the influence of ytterbium concentration in the melt on the relative concentrations of various kinds of ytterbium impurity centers, the comparative measurements of three samples with different ytterbium concentration were carried out. Magnetic properties of impurity ytterbium ions, including the probabilities of resonant transitions, are strongly anisotropic. Therefore, the measurements for all three samples were carried out at approximately the same orientation of the external magnetic field, corresponding to 35° in Fig. 3a. This orientation is marked by short vertical line. The EPR spectra of all three samples are presented in Fig. 4a. Doublet structures of the transitions are due to the presence of two magnetically nonequivalent centers. The lines marked by asterisks were used for comparison. The spectra in Fig. 4a are normalized so that the lines belonging to a single Yb ion in M1 site would be of the equal amplitude. The figure shows that the relative amplitudes of the spectral lines and, consequently, the relative concentrations of the various impurity centers depend on the total concentration of ytterbium ions. The results obtained are shown in Table 2. For each of the samples intensities of lines in the spectra were normalized relative to the integral intensity of the M1(S) line.

Comparative analysis of the data presented in Table 2 shows that increment of the total ytterbium concentration in the samples from 6.51×10^{-5} to 4.34×10^{-4} raises the content of dimeric associates relative to the concentration of the single ions in the M1 sites by factor of 2.5. At the same time, there is no clear correlation between the total concentration of ytterbium in the samples and the relative concentration of single ions in the M1 site and C3 centers. The concentration of ytterbium impurity centers also affects the line width of resonance transitions. Increase of the total ytterbium concentration leads to the doubling of line width for all the kinds of paramagnetic centers. Line width of the resonance transitions in EPR spectroscopy of low concentrated high-spin systems in crystals is determined, as a rule, by inhomogeneity of the local electric crystal field acting on the paramagnetic center. Introduction of impurity ions into crystals distorts the crystal lattice. Therefore, it is not surprising that the increase in the concentration of impurity ions increases the inhomogeneity of the crystal field. It should be noted that for all samples, the inhomogeneity of the local crystal field at the location of the ytterbium dimeric associate is about 2 times less as compared with that for the single ytterbium ions in the M1 sites. This means that the formation of neutral dimeric ytterbium associates leads to significantly less local crystal field distortion than the formation of positively charged single ytterbium ions with non-local compensation of the excess cation charge.
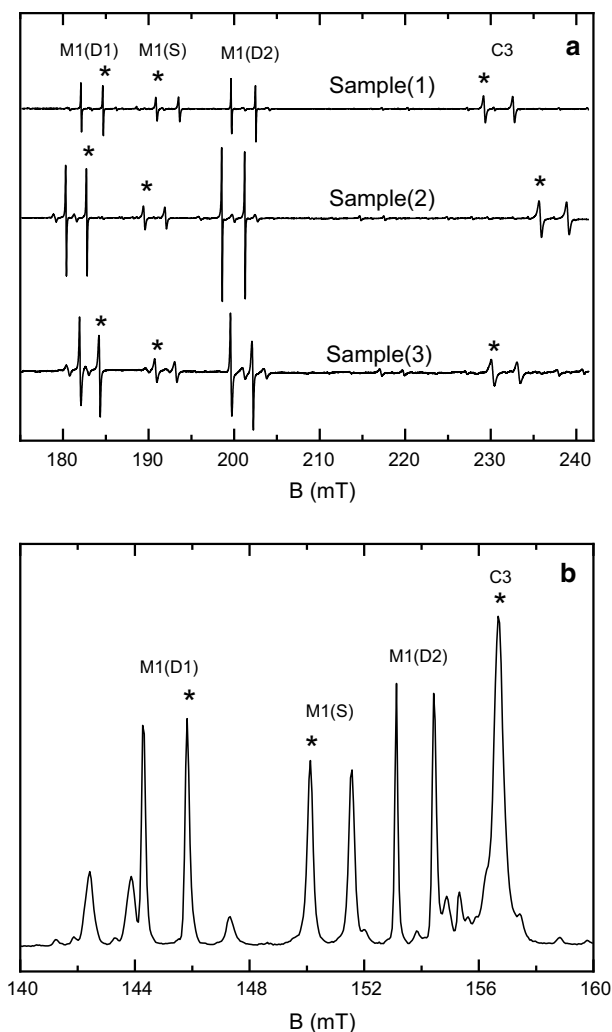
Fig. 4 EPR spectra of impurity ytterbium ions in Mg_2SiO_4 crystals. **a** continuous wave spectra of three crystals doped with ytterbium ions with different dopant concentrations. **b** spin-echo detected spectrum of the crystal grown at ytterbium concentrations in the melt of 0.15 mol.%. The designations M1(S) and M1(D) correspond to the resonance transitions of single Yb ions located in the M1 site and dimeric associates of such ions, respectively. M1(D1) and M1(D2) denote two allowed transitions between the electron levels of the spin triplet state $S = 1$ of the Yb^{3+} dimeric associates. Resonance lines with orientational dependences specific to impurity ions in the M2 site are designated as C3

4 Measurements of Relaxation Times

Relaxation measurements were carried out with the sample containing 2.08×10^{-4} at.% of ytterbium (sample 2) at the orientation of the external magnetic field corresponding to 96° in Fig. 3b. This orientation is indicated by the

**Table 2** Parameters of the resonance lines of impurity Yb^{3+} centers in Mg_2SiO_4

Sample	Resonance line	Normalized integral intensity	Line width (mT)
Sample 1 (6.51×10^{-5} at.% of Yb^{3+})	M1(S)	1.0 ± 0.1	0.21 ± 0.02
	M1(D)	0.50 ± 0.05	0.10 ± 0.01
	C3	2.5 ± 0.2	0.32 ± 0.03
Sample 2 (2.08×10^{-4} at.% of Yb^{3+})	M1(S)	1.0 ± 0.1	0.3 ± 0.03
	M1(D)	0.85 ± 0.1	0.12 ± 0.01
	C3	3.4 ± 0.3	0.42 ± 0.04
Sample 3 (4.34×10^{-4} at.% of Yb^{3+})	M1(S)	1.0 ± 0.1	0.37 ± 0.4
	M1(D)	1.25 ± 0.1	0.22 ± 0.2
	C3	2.47 ± 0.2	0.55 ± 0.5

short vertical line. Echo-detected spectrum recorded at this orientation is presented in Fig. 4b. The phase relaxation times were measured by the two-pulse sequence method with the pulse configuration $\pi/2$ ($t = 8$ ns) $- \tau - \pi$ ($t = 16$ ns). For all paramagnetic centers decay of integral echo intensity was well described by a simple one-exponential decay in the entire temperature range of 5–15 K. As an example, Fig. 5a shows the primary echo decay curve for the dimeric associate, measured at 10 K. A two-pulse electron spin-echo envelope modulation (ESEEM) is also clearly seen in this figure. Fourier analysis has shown (Fig. 5b) that this modulation is mainly due to the hyperfine interaction of the ytterbium electron spin with the nuclear spins $I = 5/2$ of ^{25}Mg isotope with the natural abundance of 10.0% and with nuclear spin $I = 1/2$ of ^{29}Si isotope with natural abundance of 7.7%. Temperature dependences of the phase relaxation times for all three kinds of the Yb^{3+} impurity centers are presented in Fig. 6a. It is seen that at temperatures $T \leq 10$ K the phase relaxation time of single Yb^{3+} ions in the M1 site is longer than that for the C3 center, but is shorter than for the dimeric associate of Yb^{3+} ions in the M1 sites.

Temperature dependences of the spin–lattice relaxation rates (SLRR) were measured by saturation-recovery method. The results are presented in Fig. 6b. To simulate temperature dependences of the SLRR ($1/T_1$), we used the expression conventional for Kramers rare-earth ions [26]

$$T_1^{-1} = A \cdot T + B \cdot T^9 + C \cdot \exp\left(-\frac{\Delta}{T}\right), \tag{3}$$

where the first term describes direct one-phonon process involving phonons with the frequency equal to the frequency of the EPR transition. The second term corresponds to the Raman two-phonon process, the third term is responsible for the processes of the two-phonon Anminov–Orbach relaxation involving the excited low-lying electron level with the energy Δ above the ground level. Results of the fitting are presented in Table 3.
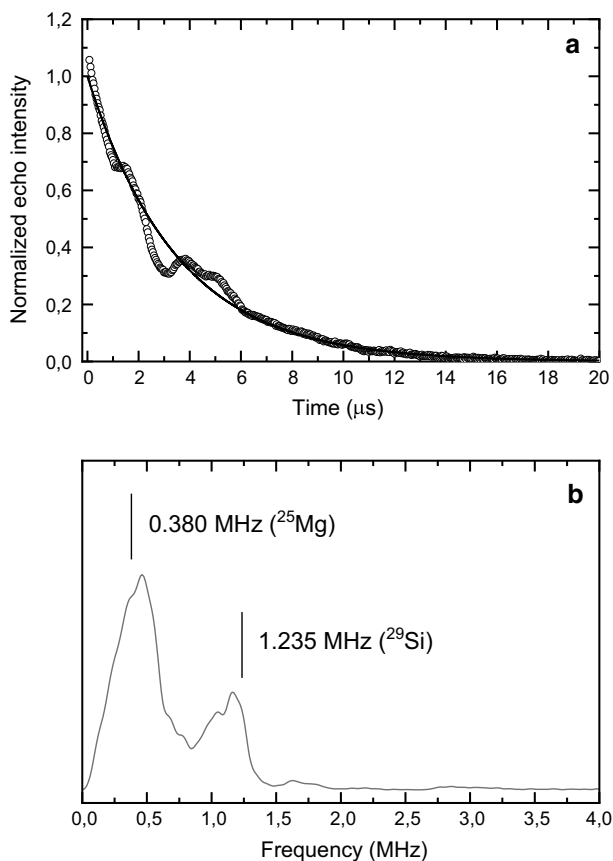
Fig. 5 a primary echo decay curve for the dimeric associate of Yb^{3+} ions in Mg_2SiO_4 Sample 2 $(2.08 \times 10^{-4}$ at.% of ytterbium). Circles are experimental data; the line is a fitting by a simple exponential decay. $T = 10$ K. **b** Fourier spectrum corresponding to the ESEEM on **a**. The vertical lines indicate the Zeeman frequencies of the ^{25}Mg and ^{29}Si nuclei

It is seen that SLRR of the single Yb^{3+} ions in the M1 site and the dimeric associate formed by Yb^{3+} ions in the M1 sites are almost the same. All three SLRR mechanisms are significantly more efficient for the C3 center than it is for the ions in the M1 sites.

We failed to find in the available literature any data on the structure of the electron levels of the ytterbium ground manifold in the Mg_2SiO_4 crystal. We can only note that obtained values of Δ do not differ significantly from the energy of the first excited electron levels of two structurally different ytterbium centers in monoclinic Y_2SiO_5 $\Delta_1 = 110$ см$^{-1}$ (158 K), $\Delta_2 = 237$ cm^{-1} (341 K) [27].

5 Discussion

1. Analysis of the presented in Table 1 principal values of the g-tensor (g_x, g_y > > g_z) shows that at arbitrary orientation of the external magnetic field the magnetic moments of Yb^{3+} ions lie close to the (xy) planes. This corresponds to the strong easy plane anisotropy of magnetic properties. The different signs of the principal values of the J-tensor indicate that spin–spin interaction between Yb ions in the dimeric associate has predominantly magnetic dipole–dipole nature. Therefore, the value and sign of the energy of spin–spin interaction should depend on orientation of the external magnetic field in respect to the crystallographic axes. It is seen in Fig. 7, where dependence of the spin–spin interaction energy on the orientation of external magnetic field in the (bc) plane is presented. This property allows one to control the energy of the spin–spin interaction between ions in the dimeric associate by changing the orientation of the external magnetic field. It may be useful for the application of ytterbium dimeric associates for quantum calculations based on coupled electron spins.

2. It is quite strange that for Yb^{3+} ions in the M1 sites and the C3 center the principal values of g-tensor are nearly the same. The only essential difference of the magnetic properties is the orientation of principal axes of the g-tensor. It means that eigenfunctions of the ground doublets of the Yb^{3+} ions in the M1 sites and C3 center are nearly the same as well. Values of Δ, characterizing the energy of the first excited electron level for the Aminov–Orbach process are also very close for the Yb^{3+} located in different crystal sites. This leads us to assume that paramagnetic center C3 with the orientation dependence, typical for the M2 site, in reality may be the dimeric associate of Yb^{3+} ions in the M1 sites with magnesium vacancy in adjacent M2 site. Structure of this associate is highlighted by dashed lines in the left side of Fig. 1. Due to strong exchange interaction between closely located Yb^{3+} ions, they lose their independence and become a single paramagnetic center with the mirror symmetry plane perpendicular to the c-axis. The orientation dependence of EPR spectra in this case should be similar to that of single paramagnetic center located in the M2 site. Then it is possible to explain the higher SLRR of the C3 center compared to the single ion and dimeric associ-

Table 3 Values of parameters in (3) determining SLRR of the Yb^{3+} impurity centers in Mg_2SiO_4

	A (s^{-1} K^{-1})	B (s^{-1} K^{-9})	C (s^{-1})	Δ (K)
Single ion (M1)	0.14	6.5×10^{-8}	7.2×10^{9}	170
Dimeric associate (M1)	0.08	1.4×10^{-7}	7.6×10^{9}	168
Center C3	0.43	8.2×10^{-7}	4.1×10^{11}	191

ate of ytterbium ions in the M1 sites. It is known that modulation of the exchange interaction by the lattice vibrations increases SLRR [28]. Very high probability of the formation of such dimeric associates is confirmed by calculations performed in Ref. [22].
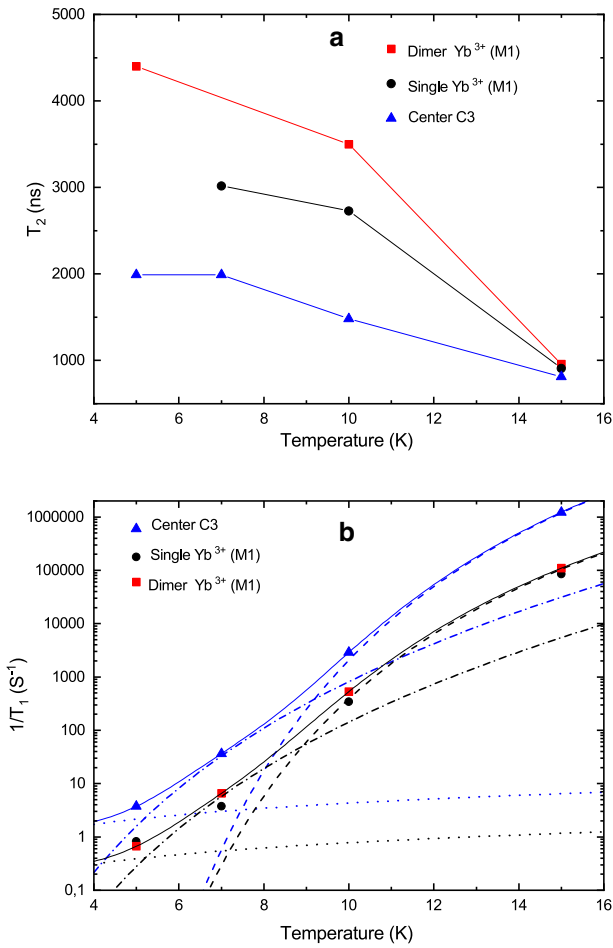
Fig. 6 **a** temperature dependences of the phase relaxation time of Yb^{3+} impurity centers in Mg_2SiO_4. **b** electron SLRR of impurity Yb^{3+} centers in Mg_2SiO_4. Lines are fittings for the single Yb^{3+} ions in both sites. Dot, dash-dot and dash lines correspond to one-phonon, two-phonon Raman and Aminov–Orbach processes. Solid lines are fits based on a model comprising all three processes

To determine the actual value of the electron spin S of the paramagnetic center, transient nutation experiments may be used [29, 30]. For the resonance transition with the change in the magnetic quantum number $\Delta m_z = \pm 1$, the frequency of the nutation ν_{nut} is determined by the expression [30]

$$\nu_{\text{nut}}\left(m_z, m_Z + 1\right) = \frac{g_1 \beta_e B_1}{h} P_{\text{Sm}} \sqrt{S(S+1) - m_z\left(m_z + 1\right)}, \tag{4}$$

where g_1 is effective g-factor for microwave magnetic field B_1, β_e is the Bohr magneton. To observe transient nutations, we used three-pulse sequences, where transient pulse of variable duration (t) was followed by a spin-echo two-pulse sequence. So transient nutations present dependence of longitudinal spin magnetization M_z on t. Results of these measurements are presented in Fig. 8. The frequencies of transient nutations for the single ion in the M1 site, dimeric associate and center 3 were determined to be 16.2, 22.4 and 19.2 MHz, respectively. During these measurements, the axis of the sample rotation was parallel to the crystal axis c (see Fig. 3b). The magnetic component of microwave field was also parallel to the crystal axis c. This orientation corresponds to the angle 157° in Fig. 3a. It is seen that at this orientation values of g_1 are nearly the same for all three centers. Therefore, the theoretical ratio of frequencies of transient nutations for the dimeric associate with effective spin $S = 1$ and single ion with effective spin $S = 1/2$ in accordance with (4) should be $\sqrt{2} \approx 1.41$. Measured ratio for the dimeric associate and single ion is about 1.38. This value is very close to the theoretical ratio. The ratio of the frequencies of transient nutations for center 3 and single ytterbium ion is about 1.18. Therefore, we cannot draw a definite conclusion about quantum number of the center 3 on the basis of these measurements.
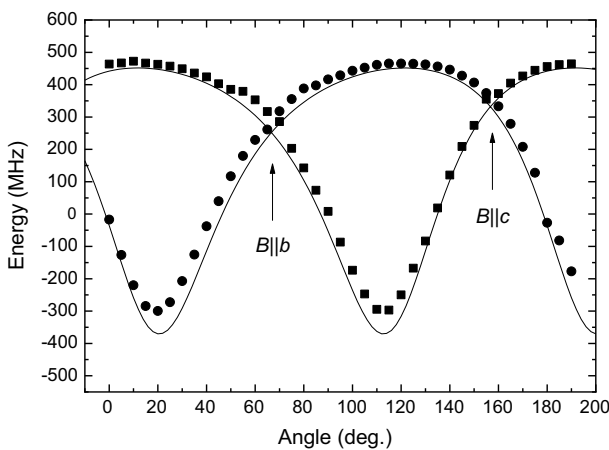

Fig. 7 Dependence of the energy of the spin–spin interaction between Yb^{3+} ions in the dimeric associate on the orientation of external magnetic field in the (bc) plane. Symbols—experiment for two magnetically nonequivalent centers, lines are fits to the spin Hamiltonian (3)

6 Conclusion

Continuous wave and pulse EPR spectroscopy was used to determine magnetic and relaxation properties of ytterbium impurity ions in Mg_2SiO_4 single crystals. Three structurally different paramagnetic centers were observed and studied. They are single Yb^{3+} ion substituting Mg^{2+} ion in the M1 site and dimer associate of Yb^{3+} ions substituting Mg^{2+} ions in two M1 sites with a magnesium vacancy in the M1 site between them. Third center may be a single Yb^{3+} ion in the M2 site or, more likely, dimer associate of Yb^{3+} ions in two nearby M1 sites with magnesium vacancy in adjacent M2 site. It was found that magnetic properties of all centers are characterized by the strong easy plane anisotropy. For the dimer associate of two Yb^{3+} ions in the M1 sites with the magnesium vacancy between them, the spin–spin interaction between Yb^{3+} ions has a predominantly dipole–dipole character. The magnitude and sign of the spin–spin interaction depend on orientation of the external magnetic field. This fact makes Yb^{3+} dimer associates in Mg_2SiO_4 promising basis for the practical implementation of elementary quantum computing algorithms on the basis of coupled electron spins.

It was found also that increment of ytterbium in the crystal raises the relative content of dimer associates there, and the formation of ytterbium associates leads to smaller disorder of local crystal electric field compared to formation of single Yb^{3+} ions with nonlocal charge compensation.

Relaxation measurements, carried out at temperatures 5–15 K showed that at low temperatures, phase relaxation times are about several µs for all the centers and increment of temperature reduces the relaxation times. Temperature dependences of the spin–lattice relaxation are well described by the joint action of the direct one-phonon process involving phonon with the frequency equal to the frequency of the EPR
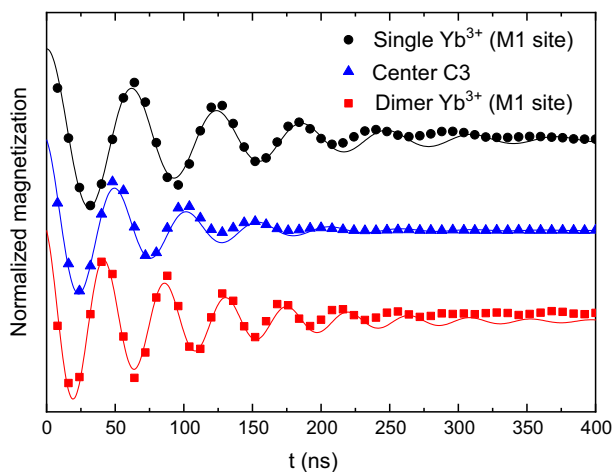
Fig. 8 Transient nutations for ytterbium impurity centers in forsterite. Black circles, red squares and blue triangles are normalized experimental data for the single Y^{3+} ion in the M1 site dimeric associate and center 3, respectively. Lines are approximations by exponentially decreasing cosines

transition, Raman two-phonon process and two-phonon resonance Aminov–Orbach process involving the excited low-lying electron level with the energy of about $125 \ cm^{-1}$.

Optical absorption spectra of Yb doped Mg_2SiO_4 crystals were measured and it was determined that the segregation coefficient of Yb impurity between crystal and melt is about 0.0009, and the optical absorption cross section for the strongest spectral line at 971 nm is about $3.8 \times 10^{-19} \ cm^2$.

References

1. H. de Riedmatten, M. Afzelius, M.U. Staudt, C. Simon, N. Gisin, Nature **456**, 773 (2008). https://doi.org/10.1038/nature076
2. C.W. Thiel, T. Böttger, R.L. Cone, J. Lumin. **131**, 353 (2011). https://doi.org/10.1016/j.jlumin.2010.12.015
3. M. Bonarota, J.-L. Le Gouët, T. Chanelière, New J. Phys. **13**, 013013 (2011). https://doi.org/10.1088/1367-2630/13/1/013013
4. C.W. Thiell, R.M. Macfarlane, Y. Sun, T. Böttger, N. Sinclair, W. Tittel, R.L. Cone, Laser Phys. **24**, 106002 (2014). https://doi.org/10.1088/1054-660X/24/10/106002
5. M. Lovrić, P. Glasenapp, D. Suter, B. Tumino, A. Ferrier, P. Goldner, M. Sabooni, L. Rippe, S. Kröll, Phys. Rev. B **84**, 104417 (2011). https://doi.org/10.1103/PhysRevB.84.104417
6. P. Jobez, C. Laplane, N. Timoney, N. Gisin, A. Ferrier, P. Goldner, M. Afzelius, Phys. Rev. Lett. **114**, 230502 (2015). https://doi.org/10.1103/PhysRevLett.114.230502
7. M. Gündoğan, P.M. Ledingham, K. Kutluer, M. Mazzera, H. de Riedmatten, Phys. Rev. Lett. **114**, 230501 (2015). https://doi.org/10.1103/PhysRevLett.114.230501
8. S. Bertaina, S. Gambarelli, A. Tkachuk, I.N. Kurkin, B. Malkin, A. Stepanov, B. Barbara, Nat. Nanotechnol. **2**, 39 (2007). https://doi.org/10.1038/nnano.2006.174
9. S. Bertaina, J.H. Shim, S. Gambarelli, B.Z. Malkin, B. Barbara, Phys. Rev. Lett. **103**, 226402 (2009). https://doi.org/10.1103/PhysRevLett.103.226402
10. J. Lehmann, A. Gaita-Arino, E. Coronado, D. Loss, Nat. Nanotechnol. **2**, 312 (2007). https://doi.org/10.1038/nnano.2007.110
11. K. Sato, S. Nakazawa, R. Rahimi, T. Ise, S. Nishida, T. Yoshino, N. Mori, K. Toyota, D. Shiomi, Y. Yakiyama, Y. Morita, M. Kitagawa, K. Nakasuji, M. Nakahara, H. Hara, P. Carl, P. Hofer, T. Takui, J. Mater. Chem. **19**, 3739 (2009). https://doi.org/10.1039/b819556k
12. F. Luis, A. Repolles, M.J. Martınez-Perez, D. Aguila, O. Roubeau, D. Zueco, P.J. Alonso, M. Evangelisti, A. Camon, J. Sese, L.A. Barrios, G. Aromi, Phys. Rev. Lett. **107**, 117203 (2011). https://doi.org/10.1103/PhysRevLett.107.117203
13. J.N. Nelson, J. Zhang, J. Zhou, B.K. Rugg, M.D. Krzyaniak, M.R. Wasielewski, J. Chem. Phys. **152**, 014503 (2020). https://doi.org/10.1063/1.5128132
14. B.Z. Malkin, A.M. Leushin, A.I. Iskhakova, J. Heber, M. Altwein, K. Moller, I.I. Fazlizhanov, V.A. Ulanov, Phys. Rev. B **62**, 7063 (2000). https://doi.org/10.1103/PhysRevB.62.7063
15. V. Mehta, D. Gourier, J. Phys. Condens. Matter **13**, 4567 (2001)
16. G.S. Shakurov, V.F. Tarasov, Appl. Magn. Reson. **21**, 597 (2001). https://doi.org/10.1007/BF03162432
17. A.V. Gaister, E.V. Zharikov, A.A. Konovalov, K.A. Subbotin, V.F. Tarasov, JETP Lett. **77**, 625 (2003). https://doi.org/10.1134/1.1600819
18. A.A. Konovalov, D.A. Lis, K.A. Subbotin, V.F. Tarasov, E.V. Zharikov, Appl. Magn. Reson. **45**, 193 (2014). https://doi.org/10.1007/s00723-013-0510-6
19. V.F. Tarasov, A.A. Sukhanov, V.B. Dudnikova, E.V. Zharikov, D.A. Lis, K.A. Subbotin, JETP Lett. **106**, 92 (2017). https://doi.org/10.1134/S0021364017140132
20. R.B. Zaripov, L.V. Mingalieva, V.F. Tarasov, E.V. Zharikov, K.A. Subbotin, D.A. Lis, Phys. Solid State **61**, 174 (2019). https://doi.org/10.1134/S106378341902032X
21. J.D. Birle, G.V. Gibbs, P.B. Moore, J.V. Smith, Am. Mineral. **53**, 807 (1968)
22. V.B. Dudnikova, E.V. Zharikov, D.A. Lis, N.N. Eremin, Phys. Solid State **61**, 614 (2019). https://doi.org/10.1134/S1063783419040097
23. J. Gale, A.L. Rohl, Mol. Simul. **29**, 291 (2003). https://doi.org/10.1080/0892702031000104887
24. V.B. Dudnikova, V.S. Urusov, E.V. Zharikov, Inorg. Mater. **41**, 627 (2005)

25. S. Stoll, A. Schweiger, J. Magn. Reson. **78**, 42 (2006). https://doi.org/10.1016/j.jmr.2005.08.013
26. A. Abragam, B. Bleaney, *Electron Paramagnetic Resonance of Transition Ions* (Clarendon Press, Oxford, 1970), pp. 565–573
27. S. Campos, A. Denoyer, S. Jandl, B. Viana, D. Vivien, P. Loiseau, B. Ferrand, J. Phys. Condens. Matter **16**, 4579 (2004). https://doi.org/10.1088/0953-8984/16/25/015
28. J.C. Gill, Proc. Phys. Soc. **79**, 58 (1962)
29. A.V. Astashkin, A. Schweiger, Chem. Phys. Letters **174**, 595 (1990). https://doi.org/10.1016/0009-2614(90)85493-V
30. A. Schweiger, G. Jeschke, *Principles of Pulse Electron Paramagnetic Resonance* (Oxford University Press, New York, 2001), p. 429